Article

Different KChIPs Compete for Heteromultimeric Assembly with Pore-Forming Kv4 Subunits

Jingheng Zhou,[1] Yiquan Tang,[2,4] Qin Zheng,[1] Meng Li,[1] Tianyi Yuan,[3] Liangyi Chen,[3] Zhuo Huang,[2] and KeWei Wang[1,2,4,*]

[1]Department of Neurobiology, Neuroscience Research Institute, Peking University Health Science Center, Beijing, China; [2]Department of Molecular and Cellular Pharmacology, PKU-IDG/McGovern Institute for Brain Research, Peking University School of Pharmaceutical Sciences, Beijing, China; [3]Institute of Molecular Medicine, Peking University, Beijing, China; and [4]Qingdao University School of Pharmacy, Qingdao, China

ABSTRACT Auxiliary Kv channel-interacting proteins 1–4 (KChIPs1–4) coassemble with pore-forming Kv4 α-subunits to form channel complexes underlying somatodendritic subthreshold A-type current that regulates neuronal excitability. It has been hypothesized that different KChIPs can competitively bind to Kv4 α-subunit to form variable channel complexes that can exhibit distinct biophysical properties for modulation of neural function. In this study, we use single-molecule subunit counting by total internal reflection fluorescence microscopy in combinations with electrophysiology and biochemistry to investigate whether different isoforms of auxiliary KChIPs, KChIP4a, and KChIP4bl, can compete for binding of Kv4.3 to coassemble heteromultimeric channel complexes for modulation of channel function. To count the number of photobleaching steps solely from cell membrane, we take advantage of a membrane tethered *k*-ras-CAAX peptide that anchors cytosolic KChIP4 proteins to the surface for reduction of background noise. Single-molecule subunit counting reveals that the number of KChIP4 isoforms in Kv4.3-KChIP4 complexes can vary depending on the KChIP4 expression level. Increasing the amount of KChIP4bl gradually reduces bleaching steps of KChIP4a isoform proteins, and vice versa. Further analysis of channel gating kinetics from different Kv4-KChIP4 subunit compositions confirms that both KChIP4a and KChIP4bl can modulate the channel complex function upon coassembly. Taken together, our findings show that auxiliary KChIPs can heteroassemble with Kv4 in a competitive manner to form heteromultimeric Kv4-KChIP4 channel complexes that are biophysically distinct and regulated under physiological or pathological conditions.

INTRODUCTION

The rapidly inactivating (A-type) potassium channels regulate membrane excitability that defines the fundamental mechanism of neural function and neurological disorders such as epilepsy. Native complexes of A-type Kv4 channels are composed of a tetrameric core of pore-forming α-subunits and additional auxiliary subunits (1,2). Binding of auxiliary subunits can change surface expression, intracellular trafficking, and gating kinetics of Kv4 channels (3–7). Cytosolic Kv channel-interacting proteins (KChIPs) that belong to a neuronal calcium sensor (NCS) family of calcium-binding EF-hand proteins coassemble with pore-forming Kv4 α-subunits to form native channel complexes that encode the somatodendritic A-type K^+ current (I_{SA}) in neurons (1,8–11). Neuronal I_{SA} plays a critical role in regulating dendritic excitability, somatodendritic signal integration, and long-term potentiation (12–16).

Auxiliary KChIP1–4 proteins represent a family of four KChIP genes with a number of isoforms in each gene subfamily. All KChIP1–4 subunits consist of a conserved C-terminal core domain with four EF-hand-like calcium-binding motifs (17), and a variable N-terminal domain that differentiates itself from others for distinct modulation on Kv4 gating (18–21). In general, KChIP1–3 increase Kv4 current amplitude, moderately slow channel inactivation and accelerate recovery from inactivation (1). KChIP4, also known as calsenilin-like protein, has six isoforms of KChIP4.1–4.6 and binds to presenilin-2 that is known to facilitate intramembranous γ-cleavage of amyloid precursor protein (22). KChIP4bl (also known as KChIP4.1) that only differs in its N-terminus with other KChIPs increases Kv4 current density, slows inactivation, and accelerates the speed of recovery from inactivation (22). In contrast, the KChIP4 splice variant KChIP4a (also known as KChIP4.4) that functions as a suppressor of Kv4 channels decreases Kv4 current density and slows open-state inactivation and recovery from inactivation (4,7,23–25). Interestingly, gene-specific alternative splicing shifts from KChIP4bl to KChIP4a that leads to inhibition of the Kv4 function can increase secretion of β-amyloid (26), suggesting a role of differential expression of KChIP isoforms and their variable subunit compositions with Kv4 in the pathogenesis of the brain such as etiology of neurodegenerations.

Submitted January 15, 2015, and accepted for publication April 20, 2015.

*Correspondence: wangkw@bjmu.edu.cn

Jingheng Zhou and Yiquan Tang contributed equally to this work.

Editor: William Kobertz.

0006-3495/15/06/2658/12 $2.00

http://dx.doi.org/10.1016/j.bpj.2015.04.024

In this study, to directly observe the number of KChIP4 subunits in Kv4.3-KChIP4 channel complexes, we used total internal reflection fluorescence (TIRF) microscopy to image fluorescent protein (FP)-tagged membrane proteins for single-molecule subunit counting (27–29). The proteins were expressed at low density in mammalian cells permitting individual channel complexes to be resolved as single fluorescent spots. By counting bleaching steps of the FP in each spot, we were able to count the number of subunits in each complex. Using two-electrode voltage clamp recordings in *Xenopus* oocytes, we further demonstrated that a variable and heteromultimeric stoichiometry of Kv4.3-KChIP4 complexes with distinct gating kinetics can be formed depending on KChIP4 expression levels.

MATERIALS AND METHODS

Plasmid constructions

For single-molecule imaging experiments, cDNAs of Kv4.3 were fused with mCherry or enhanced green fluorescent protein (EGFP), and cDNAs of KChIP4a or KChIP4bl were fused with EGFP. The C-terminal CAAX signal of *k*-ras (KKKKKKSKTKCVIM), which targets Ras proteins to the plasma membrane, was added to the C-terminus of EGFP or KChIP4a and KChIP4bl, respectively. For biochemistry experiments, cDNAs of Kv4.3 and KChIP4bl were cloned into a pEGFP-N1 vector, and KChIP4a was fused with 3×FLAG in pcDNA3.1(+) vector. A flexible 10Q (QQQQQQQQQQ) linker was introduced to link Kv4.3-Kv4.3 in tandem construct KChIP4a-2×Kv4.3. For two-electrode voltage clamp recordings of *Xenopus* oocytes, Kv4.3, KChIP4a, KChIP4bl, and tandem cDNA constructs were transferred into a pBluescript KSM vector for functional expression.

Confocal microscopy

HEK 293 cells were maintained at 37°C under 5% CO_2 in Dulbecco's modified Eagle medium supplemented with 10% fetal bovine serum. For confocal imaging, cells were reseeded on glass coverslips coated with poly-D-lysine for detection. Cells were transfected with cDNA constructs using Lipofectamine 2000 (Invitrogen, Grand Island, NY) following the manufacturer's instructions. After 24–48 h of transfection, cells were washed three times with phosphate buffered saline and fixed in 4% paraformaldehyde at 4°C for 15 min. Images were obtained using a confocal microscope (FV1000, Olympus, Beijing, China).

Imaging of single molecules

TIRF reflection images were collected with fixed cells. GFP was excited with a 473 nm laser, and mCherry was excited with a 561 nm laser. Laser power of ~6 mW was applied to the rear pupil of an oil objective (Olympus 150X, N.A. = 1.45). To reduce background noise and maximize emission, photons were detected by using a back-illuminated electron-multiplying charge-coupled device (EMCCD) camera (Andor iXon DV-888 BV) and high quality filters (Chroma (Bellows Falls, VT), 49002 ET-GFP and 49009 ET-mCherry). In addition, a laser blocker absorbed the reflected laser beam at the rear pupil of the objective. We set the gain of our EMCCD camera at 300 throughout all single-molecule imaging experiments. These settings were in the linear dynamic range of the EMCCD camera. Measurements were made from the illumination field of the TIRF microscope to evaluate its heterogeneity. Because the intensity at the edge of the excitation field was at least 85% of that at the center, we treated the illumination as a relatively homogeneous field. The output of the camera is measured in counts from its 14-bit analog-to-digital (A/D) converter, and the manufacturer's equation was used to convert from counts to photons (photoelectrons) collected during the 200 ms sampling period as follows:

$$P = \frac{S \times T_{A/D}}{G},$$

where P is the number of photons, S is the observed fluorescence intensity (counts), $T_{A/D}$ is the conversion factor to convert EMCCD counts to photoelectrons (10.5 electrons per A/D count at unity gain), and G is the EMCCD gain (28).

Imaging analysis

Movies of 1000 frames of a 25 pixel area (87 × 87 nm per pixel) were acquired with 5 frames per second. Fluorescence from mCherry was recorded for 50 s under illumination with 561 nm light. After most mCherry fluorescent spots were bleached out, 561 nm light was switched off and subsequently 473 nm light was turned on before GFP fluorescence was recorded. We subtracted the background fluorescence using the rolling ball method in Image J (National Institutes of Health (NIH)). Because the noise in images was high, we determined the center of mass of each fluorescence punctum using an algorithm written in MATLAB (The MathWorks, Natick, MA) developed previously (27,28). The algorithm averaged the first 5–10 frames of the fluorescence signal, and then applied a threshold to obtain connected regions of interest (ROIs) above that threshold. The threshold was set at 10 times the SD measured in an area with no cells. ROIs smaller than 3 pixels were regarded as noise and discarded. ROIs with areas larger than 15 pixels were segmented by Gaussian fitting, and multiple peaks that were very close were excluded. Centroid analysis or nonlinear Gaussian fitting algorithms was used to find the peaks of ROIs in the averaged image. We obtained the summed fluorescence intensity in a square region of 5 × 5 pixels that enclosed a peak. These methods yielded almost identical results to subpixel resolution, as explained and used previously by others and our studies (27,28). The time course was plotted to identify the bleaching steps of that spot. Subsequently, bleaching transitions were scored manually by one investigator and rescored blindly by another. Apparent variance changes and step size were included in the scoring criteria. Traces receiving inconsistent scoring and traces with erratic behavior of the total fluorescence were rejected. The fraction of KChIP4s-EGFP-CAAX and Kv4.3-mCherry incidentally falling within a diffraction-limited spot without being associated was calculated by the formula: $f = a \times d_g \times d_r / (d_g + d_r)$, where $a = \pi \times r^2$ is the area of the disk around a spot with $r = 150$ nm, d_g and d_r the green and red spot densities (measured using Image J, NIH, Bethesda, MD), and f the resulting fraction of overlapping spots (29).

Electrophysiological recordings

For whole-cell patch clamp recordings in HEK 293 cells, currents were recorded at room temperature using an EPC 10 USB amplifier with PatchMaster software (HEKA Electronics, Bellmore, NY). Patch electrodes were pulled from borosilicate glass and fire-polished to a resistance of 2–4 megaohms. The bath solution contained 135 mM NaCl, 2.5 mM KCl, 10 mM HEPES, 1 mM $MgCl_2$, 1.5 mM $CaCl_2$, and 10 mM glucose at pH 7.4, and the pipette solution contained 135 mM potassium gluconate, 10 mM KCl, 10 mM HEPES, 1 mM $CaCl_2$, 1 mM $MgCl_2$, and 10 mM EGTA at pH 7.3.

For two-electrode voltage clamp recordings in oocytes, all cRNAs were transcribed in vitro from linearized plasmids in pBluescript KSM vectors by using the T3 mMESSAGEmMACHINE Kit (Ambion, Grand Island, NY). *Xenopus laevis* oocytes (stage V-VI) were injected with 46 nl of cRNA solution, containing 0.5–5.0 ng of cRNA, using a microinjector

(Drummond Scientific, Broomall, PA). Oocytes were then kept at 17°C in ND96 solution (96 mM NaCl, 2 mM KCl, 1.8 mM $CaCl_2$, 1 mM $MgCl_2$, 5 mM HEPES, pH 7.4, adjusted with NaOH). 1 to 2 days after injection, oocytes were impaled with two microelectrodes (0.5–1.0 megaohms) filled with 3 M KCl in a 40-μl recording chamber. Currents were recorded in ND96 solution at room temperature using a GeneClamp 500B amplifier (Axon Instruments, Sunnyvale, CA).

Data were acquired using PatchMaster software (HEKA) and digitized at 1 kHz with an LIH 8 + 8 computer interface (HEKA). OriginPro version 8.6 (OriginLab, Northampton, MA) was used to analyze the data. To measure the peak current amplitudes and the kinetics of open-state inactivation, the currents were evoked by a 2-s depolarizing pulse to +40 mV from a holding potential of −100 mV. The time constants of macroscopic inactivation were obtained by curve fitting with a single exponential function. Recovery from inactivation was monitored with a double-pulse protocol in which the current was evoked by a test pulse of +40 mV from −100 mV (I_{pre}) and from subsequent −100 mV holding potential of variable durations from 5 ms to 1.285 s (I_{post}). Normalized currents for recovery were determined as the ratio of I_{post}/I_{pre}. The kinetics of recovery was obtained by fitting the normalized current amplitudes as a function of −100 mV duration. Steady-state inactivation (SSI) was assessed by determining the peak current amplitudes at +40 mV after 5-s prepulses ranging from −120 to 0 mV. The voltage dependence of SSI (I/I_{max}) was fitted to the following single Boltzmann relationship, $y = 1/(1 + \exp((V - V_{1/2})/k))$, where V is the test potential, $V_{1/2}$ is the potential for half-maximal inactivation, and k is the corresponding slope factor. Closed-state inactivation (CSI) was monitored with a double-pulse protocol in which the current was evoked by a test pulse of +40 mV from −100 mV (I_{pre}) and from subsequent −50 mV prepulses of variable durations from 5 ms to 10.4 s (I_{post}). Normalized currents for CSI were determined as the ratio of I_{post}/I_{pre}. The kinetics of CSI was obtained by fitting the normalized current amplitudes as a function of prepulse duration. All holding potentials were −100 mV in this study unless specified.

Coimmunoprecipitation and Western blot assay

Transfected HEK 293 cells were washed three times with ice cold phosphate buffered saline. Cells were lysed with lysis buffer (150 mM NaCl, 20 mM Tris, 1% Triton X-100, 1% sodium deoxycholate, 0.1% sodium dodecyl sulfate, 10 mM EDTA, and proteinase inhibitor mixture (Roche Applied Science, Shanghai, China), pH 8.0) at 4°C for 30 min. The cell lysates were then centrifuged at 13,000 × g for 10 min to yield the protein extract in the supernatant. One fraction containing 200 μg of protein was incubated with 1–2 μl resin (Sigma, St. Louis, MO) for 5 h or overnight at 4°C to immunoprecipitate the FLAG fusion protein, and the other fraction was prepared as input protein. After incubation, the resin-binding FLAG fusion proteins were washed four times with Tris buffered saline and eluted with 0.1 M glycine HCI, pH 3.5. The input and IP proteins were both subjected to Western blot analysis.

For Western blot assays, protein samples were loaded on 10% sodium dodecyl sulfate polyacrylamide gel electrophoresis and transferred using gel electrophoresis to nitrocellulose membranes (Millipore, Billerica MA). After blocking, nitrocellulose membranes were incubated with rabbit monoclonal anti-EGFP (1:2000; Abcam, Cambridge, MA), or mouse monoclonal anti-FLAG (1:4000; Sigma) at 4°C overnight. The membranes were then incubated with their corresponding secondary horseradish peroxidase-conjugated antibodies and detected using an ECL Western blotting detection system (Millipore).

Statistics

For electrophysiological recordings, curve fittings were performed with OriginPro version 8.6 (Microcal Software, Northampton, MA). Data were expressed as mean ± SE. Statistical analysis was conducted by Student's t-test for quantitative analysis for peak current amplitudes and inactivation time constants (Prism 5, GraphPad Software, San Diego, CA). The statistical significance was considered as $^{**}p < 0.01$; $^{***}p < 0.001$.

RESULTS

Tetrameric assembly of pore-forming Kv4.3 α-subunits

To optimize the fluorescence signal detected by single-molecule subunit counting, we started with examining the subunit stoichiometry of Kv4.3 fused with EGFP in the channel C-terminus (Kv4.3-EGFP) and expressed in HEK 293 cells (Fig. 1 *A*). Examining the tetrameric α-subunit Kv4.3 serves as a positive control to confirm the validity of the subunit counting by single-molecule imaging (27,30). The cells were fixed before the counting to prevent any fluorescence fluctuation induced by the lateral movement of fusion proteins. The expression of Kv4.3-EGFP gave rise to a punctate appearance of fluorescence on the surface membrane visualized by TIRF microscopy at high gain (Fig. 1 *A*), indicating the single Kv4.3 channel complexes formed. Photobleaching by applying a defined continuous laser power to the cells induced a stepwise loss of the fluorescent spots (Fig. 1 *B*). For each of the chosen fluorescent spots, a number of bleaching steps was counted to determine the number of fluorescent GFP molecules that the channel contained, as previously described for studies of other ion channels (27,28). Because the EGFPs are likely not always fluorescent, perhaps due to misfolding or incomplete maturation, or endogenous Kv4 channels, there are not always four bleaching steps from a single fluorescent spot, even for the tetrameric Kv4 channel. The distribution of the photobleaching steps was fitted by a binomial distribution formula with a probability (p) of EGFP being fluorescent as a free parameter. We collected 223 countable spots for Kv4.3-EGFP from cells and analyzed the photobleaching events for subunit stoichiometry. The results showed a well fit of distributions by a binomial distribution with $p = 80\%$ (Fig. 1 *C*) (27,28), representing four Kv4.3 subunits in the channel.

Variable subunit stoichiometry of octameric Kv4.3-KChIP4 complexes

Previous structural efforts of ours and others reveal that a single KChIP molecule laterally clamps two neighboring Kv4.3 in a 4:4 manner (31,32). To confirm this stoichiometry and further explore whether different KChIPs can competitively bind to Kv4.3 in situ, we used the single-molecule subunit counting assay to visualize Kv4/KChIPs stoichiometry with various ratios of Kv4 and KChIP4 isoforms in mammalian HEK 293 cells. Coexpression of KChIP4a with Kv4.3 resulted in cytoplasmic localization of Kv4.3-KChIP4a complexes (Fig. 2 *A*), consistent with the characteristic of KChIP4a that causes endoplasmic reticulum retention of Kv4.3 (4,6,7). Similarly, coexpression of

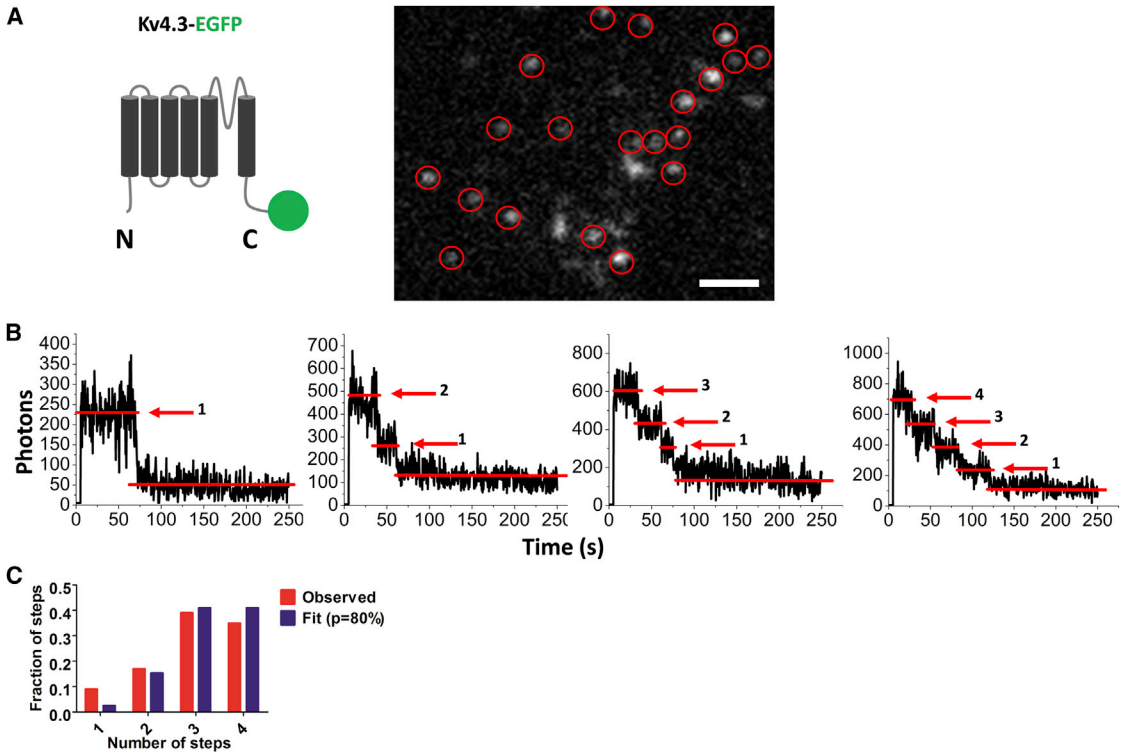

FIGURE 1 Pore-forming Kv4.3 α-subunit forms a tetramer. (*A*) Schematic illustration of the Kv4.3-EGFP (*left*). Representative image (*EGFP channel*) taken using TIRF microscopy shows the Kv4.3 puncta on the plasma membrane of a fixed HEK 293 cell (*right*). The puncta enclosed with red circles were chosen for later single-molecule bleaching analysis (Scale bar: 1 μm). (*B*) Examples of photon traces from example spots with one, two, three, or four GFP bleaching steps (marked by *red arrowheads*). Representative time courses of GFP emission are shown after background correction. The *y* axis plots the photons collected per 200-ms sampling period for comparison. Red lines mark the photon levels. (*C*) Histogram of bleaching steps for GFP (*red*) from cells expressing Kv4.3-EGFP and the fit with 80% probability ($p = 80\%$) of GFP being fluorescent (*blue*) ($n = 223$ spots).

KChIP4bl with Kv4.3 gave rise to cytoplasmic and plasma membrane distribution of Kv4.3-KChIP4bl complexes (Fig. 2 *C*). The TIRF microscopy is able to visualize intracellular events occurring >100 nm from the membrane surface, which can acquire fluorescent signals of unbound KChIP4 proteins from cytosol and endoplasmic reticulum, thus leading to excessive photobleaching step counting. To count the number of photobleaching steps solely from the cell membrane, we took advantage of a membrane tethered *k*-ras-CAAX peptide (KKKKKKSKTKCVIM) from mammalian *k*-Ras proteins (33,34). The *k*-ras-CAAX sequence was appended to the C-terminus of KChIP4a-EGFP or KChIP4bl-EGFP proteins (KChIP4a-EGFP-CAAX or KChIP4bl-EGFP-CAAX) that can anchor either unbound KChIP4 proteins or Kv4.3-KChIP4 complexes to the plasma membrane for the reduction of background noise (Fig. 2, *B* and *D*). To test whether the *k*-ras-CAAX sequence had any effects on channel properties, we recorded and compared the whole-cell currents that resulted from coexpression of either Kv4.3-mCherry + KChIP4a-EGFP or Kv4.3-mCherry + KChIP4a-EGFP-CAAX in HEK 293 cells (Fig. 2 *E*). Like the coexpression of Kv4.3-mCherry + KChIP4a-EGFP, coexpression of Kv4.3-mCherry + KChIP4a-EGFP-CAAX revealed similar inactivation time constants (τ_{inact}) with 286.5 ± 27.8 ms ($n = 10$) and voltage-dependent SSI ($V_{1/2}$) with −62.5 ± 0.4 mV ($n = 9$), as compared with Kv4.3-mCherry + KChIP4a-EGFP for τ_{inact} at 270.4 ± 23.2 ms ($n = 10$) (Fig. 2 *F*) and for $V_{1/2}$ at −63.6 ± 0.5 mV ($n = 9$) (Fig. 2 *G*). This result indicates that coexpressing *k*-ras-CAAX sequence had no effect on channel gating properties, thus allowing us to further investigate whether different KChIP4s can compete for binding to Kv4.3.

Cotransfection of Kv4.3-mCherry with KChIP4a-EGFP-CAAX or KChIP4bl-EGFP-CAAX at 1:1 ratio in HEK 293 cells gave rise to surface expression of the channel complexes when excited with 561 nm laser for mCherry (Kv4.3) and 473 nm laser for GFP (KChIP4s). To identify KChIP4a or KChIP4bl that was associated with Kv4.3 subunits, we merged the red and green images (Fig. 3 *A*), and identified GFP spots that overlapped with mCherry spots (*green circles* in Fig. 3 *A*). For each of the overlapped fluorescent spots, the number of bleaching steps was counted to determine the number of fluorescent mCherry and GFP molecules within the channel complexes from either Kv4.3-KChIP4a or Kv4.3-KChIP4bl (Fig. 3 *B*) (29,35).

Consistent with the cocrystal structure of Kv4.3N-KChIP1 (31), the results showed that both KChIP4a and

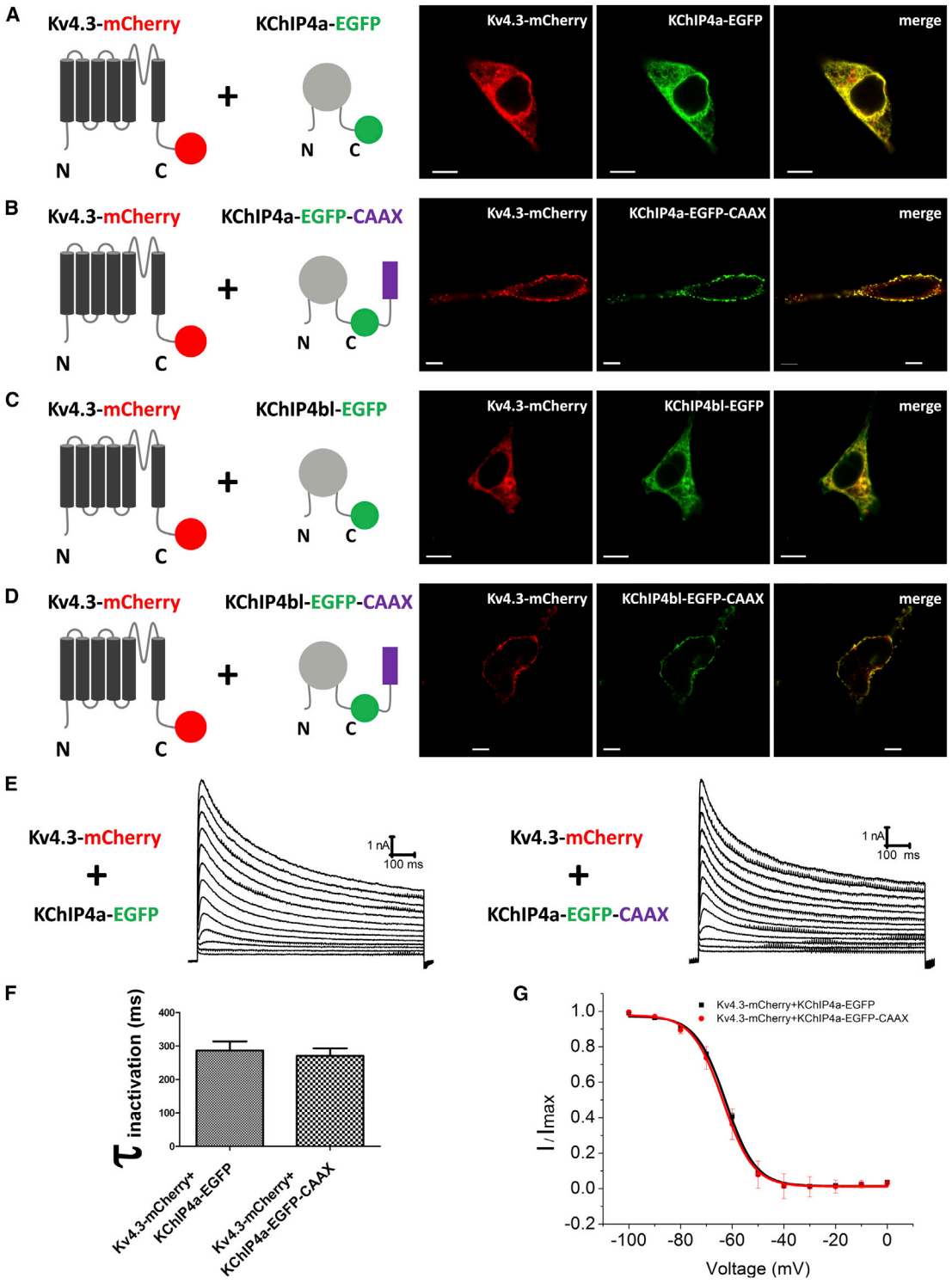

FIGURE 2 The anchor of KChIP4a and KChIP4bl to the plasma membrane by CAAX membrane-tethered signal peptide. (*A*) Cytoplasmic distributions of Kv4.3-mCherry and KChIP4a-EGFP. (*B*) Plasma membrane distributions of Kv4.3-mCherry and KChIP4a-EGFP-CAAX. (*C*) Cytoplasmic and plasma membrane distributions of Kv4.3-mCherry and KChIP4bl-EGFP. (*D*) Plasma membrane distributions of Kv4.3-mCherry and KChIP4bl-EGFP-CAAX. –CAAX indicates attachment of a PM-targeting CAAX signal from *k*-Ras to the C-terminus of fusion proteins (Scale bars: 10 μm). Schematic illustrations of constructs used for coexpression are shown in the left panels. (*E*) Representative current traces of Kv4.3-mCherry + KChIP4a-EGFP (*left*) and Kv4.3-mCherry + KChIP4a-EGFP-CAAX (*right*) expressed in HEK 293 cells. (*F*) Quantitative analysis of inactivation time constants for Kv4.3-mCherry + KChIP4a-EGFP and Kv4.3-mCherry + KChIP4a-EGFP-CAAX ($n = 10$ cells). Values are mean ± SE. Statistical analysis was conducted by Student's *t*-test, and the statistical significance was considered as $p > 0.05$. (*G*) Quantitative analysis of the voltage dependence of SSI of Kv4.3-mCherry + KChIP4a-EGFP and Kv4.3-mCherry + KChIP4a-EGFP-CAAX ($n = 9$ cells).

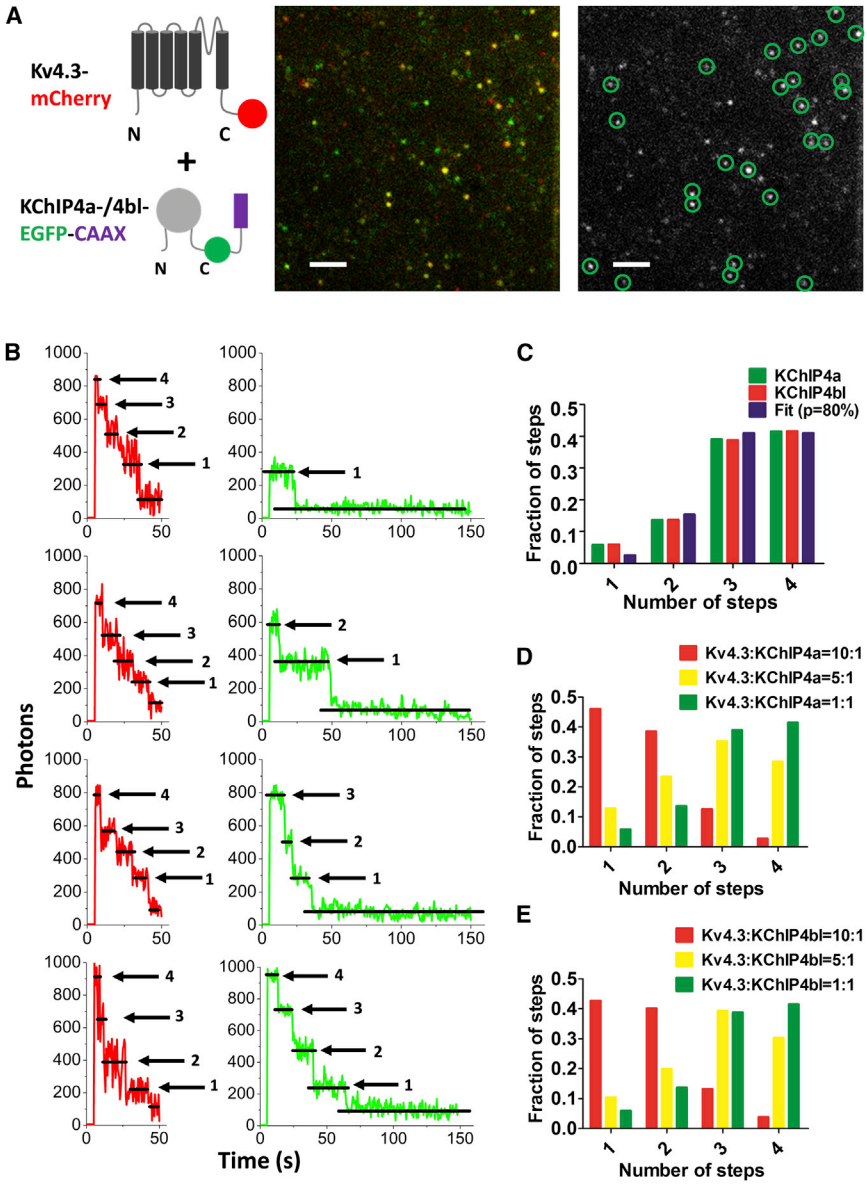

FIGURE 3 The formation of variable stoichiometry of Kv4.3-KChIPs channel complexes is dependent on the relative expression level of auxiliary KChIP4a or KChIP4bl proteins. (*A*) Schematic illustration of Kv4.3-mCherry and KChIP4a-/KChIP4bl-EGFP-CAAX (*left*). Overlay of mCherry image with Kv4.3-mCherry spots and GFP image with KChIP4a-EGFP-CAAX or KChIP4bl-EGFP-CAAX spots from HEK 293 cell (*middle*). Overlapping spots are circled in green in GFP image (*right*). (Scale bar represents 2 μm). (*B*) Examples of photon traces from example spots with one, two, three, or four GFP bleaching steps (marked by *black arrowheads*). Black lines mark photon levels. (*C*) Histogram of bleaching steps for GFP from cells expressing Kv4.3-mCherry and KChIP4a-EGFP-CAAX (*green*) or KChIP4bl-EGFP-CAAX (*red*) (2 and 2 μg), and the fit with 80% probability of GFP being fluorescent (*blue*) (n = 205, 219 spots). (*D*) Distributions of numbers of GFP bleaching steps from KChIP4a-EGFP-CAAX with the ratios of Kv4.3 and KChIP4a as indicated (n = 205–215 spots). (*E*) Distributions of numbers of GFP bleaching steps from KChIP4bl-EGFP-CAAX with the ratios of Kv4.3 and KChIP4bl as indicated (n = 219–234 spots).

KChIP4bl can assemble with Kv4.3 to form channel complexes in a 4:4 manner (Fig. 3 *C*). To further test whether variable expression levels of KChIP4a or KChIP4bl can have any effect on the subunit composition, cells were cotransfected with Kv4.3-mCherry and KChIP4a-EGFP-CAAX (or KChIP4bl-EGFP-CAAX) at different ratios of 1:1, 5:1, and 10:1. The GFP bleaching (KChIP4a or KChIP4bl) was counted exclusively from spots that overlapped with red fluorescent spots (Kv4.3). As the relative expression level of Kv4.3 over KChIP4a or KChIP4bl increased, the number of bleaching steps decreased (Fig. 3, *D* and *E*). To test whether the *k*-ras-CAAX sequence had any artificial effect on stoichiometry of KChIP4s, we used empty vector mCherry as a negative control and tested the effect of mCherry at different ratios of 1:1, 5:1, and 10:1 (mCherry:KChIP4-EGFP-CAAX) on bleaching steps of EGFP (KChIP4a or KChIP4bl). The result showed that the bleaching steps of either KChIP4a or KChIP4bl remained unchanged (Fig. S1 in the Supporting Material). We collected 7548 countable green spots from 47 cells in total. 3145 out of 7548 green spots (41.7%) were overlapped with red spots. We also calculated the fraction of KChIP4s-EGFP-CAAX and Kv4.3-mCherry that might incidentally fall within a diffraction-limited spot without being associated (29).The fraction of incidental red/green colocalization (f) was ranged from 0.5% to 5.6%, with an average of 2.3 $\pm$ 0.7% (n = 47 cells), significantly below the fraction of observed colocalization from overlapped spots. These results indicate that binding of Kv4.3 and KChIP4a or KChIP4bl can vary ranging from 4:1 to 4:4 (Kv4.3:KChIP4) and the stoichiometry of Kv4.3-KChIP4 complexes is dependent upon their relative expression levels.

Competitive binding to and modulation of Kv4.3 by KChIP4a and KChIP4bl

To examine whether distinct KChIP4s can compete for binding to Kv4.3 channels, we fused KChIP4a and KChIP4bl with 3×FLAG (KChIP4a-3×FLAG) and EGFP (KChIP4bl-EGFP), respectively, and Kv4.3 with EGFP (Kv4.3-EGFP) in their C-terminus (Fig. 4 *A*). HEK 293 cells were either dual-transfected with KChIP4a-3×FLAG and KChIP4bl-EGFP, or triple-transfected with KChIP4a-3×FLAG, KChIP4bl-EGFP, and Kv4.3-EGFP. As a negative control, HEK 293 cells were triple-transfected with 3×FLAG, KChIP4bl-EGFP, and Kv4.3-EGFP (Fig. 4 *A*). Cell lysates were incubated with anti-FLAG affinity gel resin for 5 h or overnight. After eluted with glycine HCl, the purified samples and input proteins were separated by sodium dodecyl sulfate polyacrylamide gel electrophoresis and Western-blotted with either anti-FLAG or anti-EGFP antibody. The results showed that KChIP4bl can be precipitated by KChIP4a only when coexpressed with Kv4.3, indicating that KChIP4bl and KChIP4a do not directly interact, and both KChIP4a and KChIP4bl can bind to Kv4.3 to form ternary complexes (Fig. 4 *A*). This ternary complex makes it possible that both KChIP4a and KChIP4bl compete for common KChIP-binding sites in tetramer Kv4.3 channel.

To further test whether both KChIP4a and KChIP4bl can competitively heteroassemble with Kv4.3 channel, HEK-293 cells were triple-transfected with Kv4.3-mCherry and KChIP4a-EGFP-CAAX at 1:1 ratio, and together with increasing amounts of KChIP4bl-CAAX cDNA at the ratio of 1:1, 1:5, and 1:10 for KChIP4a over KChIP4bl (Fig. 4 *B*). As described earlier, we counted the number of bleaching steps for each of the overlapped fluorescent spots to determine the subunit compositions of the channel complexes.

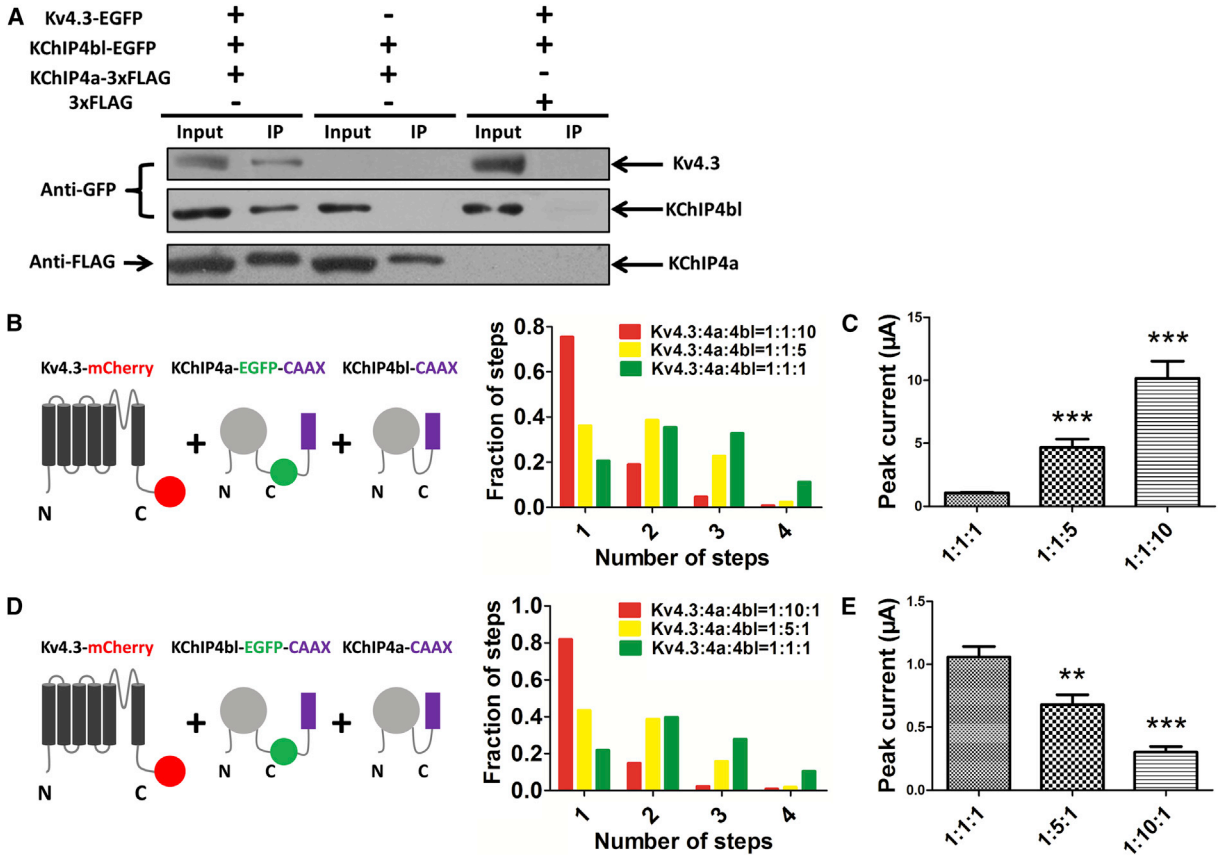

FIGURE 4 Different KChIP subunits competitively bind to Kv4.3 channels. (*A*) HEK 293 cells were transfected with constructs indicated on top of each panel. Immunoprecipitations were carried out with anti-FLAG antibodies that recognize KChIP4a-3×FLAG, followed by Western blotting to detect Kv4.3 or KChIP4bl. GFP-tagged Kv4.3 and KChIP4bl proteins were detected with antibody against GFP. (*B*) Schematic illustration of Kv4.3-mCherry, KChIP4a-EGFP-CAAX, and KChIP4bl-CAAX (*left*). Distributions of numbers of GFP bleaching steps from KChIP4a-EGFP-CAAX for different ratios of KChIP4a and KChIP4bl as indicated ($n = 209$–246 spots) (*right*). (*C*) Quantitative analysis for enlargement of Kv4-KChIP complex current by KChIP4bl in a dose-dependent manner ($n = 11$–15 oocytes). Values are mean ± SE. Statistical analysis was conducted by Student's *t*-test, and the statistical significance was considered as $^{***}p < 0.001$. (*D*) Schematic illustration of Kv4.3-mCherry, KChIP4a-CAAX, and KChIP4bl-EGFP-CAAX (*left*). Distributions of numbers of GFP bleaching steps from KChIP4bl-EGFP-CAAX for different ratios of KChIP4a and KChIP4bl as indicated ($n = 201$–222 spots) (*right*). (*E*) Quantitative analysis for suppression of Kv4-KChIP channel complex current by KChIP4a in a dose-dependent manner ($n = 9$–15 oocytes). Values are mean ± SE; $^{**}p < 0.01$; $^{***}p < 0.001$. To see this figure in color, go online.

As shown in Fig. 4 *B*, with a fixed coexpression ratio (1:1) between Kv4.3-mCherry and KChIP4a-EGFP-CAAX, increasing KChIP4bl (KChIP4bl-CAAX) expression yielded a dose-dependent reduction of KChIP4a-EGFP bleaching steps. This indicates a competition between KChIP4bl and KChIP4a for binding to Kv4.3. Reciprocally, increasing KChIP4a (KChIP4a-CAAX), with a fixed ratio (1:1) between Kv4.3-mCherry and KChIP4bl-EGFP-CAAX, yielded a dose-dependent reduction of KChIP4bl-EGFP bleaching steps (Fig. 4 *D*).

To functionally confirm the competitive binding between KChIP4a and KChIP4bl for Kv4.3, we coinjected Kv4.3 with a variable ratio of KChIP4a over KChIP4bl cRNAs in oocytes. The current of Kv4.3-KChIP4 complex was either enhanced by KChIP4bl (Fig. 4 *C*), or inhibited by KChIP4a (Fig. 4 *E*) in a dose-dependent manner. These results indicated that KChIP4a and KChIP4bl could functionally compete for coassembly with Kv4.3 to form channel complexes and modulate channel function, which was dependent upon either KChIP4a or KChIP4bl expression level.

Gating properties of Kv4.3-KChIP4 complexes

To further confirm whether the functional properties of the channel complexes were affected by variable KChIP4 expressions, we generated two tandem constructs in which one KChIP4a subunit was attached to a tandem Kv4.3 (KChIP4a-2×Kv4.3) to mimic the subunit ratio of 4:2 for Kv4.3 over KChIP4a; and one KChIP4a subunit attached to one Kv4.3 subunit (KChIP4a-Kv4.3) to mimic the 4:4 ratio (Kv4.3 over KChIP4a). For easy analysis of gating properties of Kv4.3-KChIP4 complexes, we injected Kv4.3 alone or tandem Kv4.3 with KChIP4a (KChIP4a-2×Kv4.3) into *Xenopus laevis* oocytes for functional expressions (Fig. 5 *A*, *left panels*). The peak currents of Kv4.3 coexpressed with two or four KChIP4a were significantly reduced in a KChIP4a-dependent manner, as compared with Kv4.3 alone (Fig. 5 *A*, *right panel*, and Table 1), consistent with literature for KChIP4a that reduces Kv4 current (7). In contrast, coexpression of tandem Kv4.3 and KChIP4a complex with KChIP4bl that functions like KChIP1 (22), the current of channel complex was increased to 5.8 ± 0.1 μA (n = 24), as compared with tandem Kv4.3 and KChIP4a coexpressed with KChIP4a (1.4 ± 0.1 μA, n = 20) or tandem Kv4.3 and KChIP4a complex (3.0 ± 0.1 μA, n = 30), indicating both KChIP4a and KChIP4bl can modulate Kv4.3 by competitively binding to Kv4.3 channels (Fig. 5 *B* and Table 1).

The gating kinetic is another functional feature that reflects coassembly of channel complexes. The analysis of inactivation time constant further confirmed that a slow inactivation was observed in the group of two KChIP4a subunits (KChIP4a-2×Kv4.3) with τ_{inact} = 269.2 ± 7.3 ms (n = 18), and a further reduction of inactivation rate was seen in the channel complexes with four subunits of KChIP4a (KChIP4a-Kv4.3) with τ_{inact} = 624.4 ± 7.8 ms (n = 14), as compared with Kv4.3 alone (τ_{inact} = 40.3 ± 2.5 ms, n = 30) (Fig. 5 *C*, *right panel* and Table 1). In contrast, coexpression of KChIP4bl resulted in a faster inactivation (τ_{inact} = 123.6 ± 4.2 ms, n = 18) of KChIP4a-2×Kv4.3 (Fig. 5 *C*, *right panel*, and Table 1). The change for speed of recovery from inactivation followed the same order, in which the recovery from inactivation for KChIP4a-saturated KChIP4a-Kv4.3 (τ_{rec} = 160.1 ± 16.3 ms, n = 17) is slower than KChIP4a-2×Kv4.3 (τ_{rec} = 145.2 ± 28.6 ms, n = 13), as compared with Kv4.3 (τ_{rec} = 94.1 ± 12.3 ms, n = 17) (Fig. 5 *D*, *right panel*, and Table 1). The speed of recovery from inactivation for the saturated KChIP4a group (KChIP4a-2×Kv4.3 coexpressed with KChIP4a) is slow with τ_{rec} = 160.2 ± 3.4 ms (n = 10), as compared with unsaturated KChIP4a-2×Kv4.3 (τ_{rec} = 145.2 ± 28.6 ms, n = 13). In contrast, coexpression of KChIP4bl with KChIP4a-2×Kv4.3 resulted in an increase of recovery rate with 61.2 ± 6.8 ms (Fig. 5 *D*, *right panel*, and Table 1).

We also examined the voltage dependence of SSI of these channels and found that KChIP4a shifted the inactivation curves in a hyperpolarization direction for KChIP4a-Kv4.3 ($V_{1/2}$ = −63.3 ± 0.8 mV, n = 10) and for KChIP4a-2×Kv4.3 ($V_{1/2}$ = −60.6 ± 1.1 mV, n = 15), as compared to Kv4.3 ($V_{1/2}$ = −53.7 ± 0.9 mV, n = 30) (Fig. 5 *E*, *right panel*, and Table 1). Coexpression of KChIP4a with KChIP4a-2×Kv4.3 shifted the inactivation curve in a hyperpolarization direction with $V_{1/2}$ = −63.4 ± 0.7 mV (n = 15) and coexpression of KChIP4bl shifted the inactivation curve of KChIP4a-2×Kv4.3 complexes to the opposite depolarization direction with $V_{1/2}$ = −54.9 ± 0.3 mV (n = 23), as compared with $V_{1/2}$ = −60.6 ± 1.1 mV (n = 15) for KChIP4a-2×Kv4.3 alone (Fig. 5 *E*, *right panel*, and Table 1). CSI is another gating property to evaluate the effect of KChIP4a on Kv4.3 (7). KChIP4a increased the rate of CSI for KChIP4a-Kv4.3 (KChIP4a-saturated, $\tau_{inact,CSI}$ = 1957 ± 119 ms, n = 12) is faster than KChIP4a-2×Kv4.3 (KChIP4a-half occupied, $\tau_{inact,CSI}$ = 2354 ± 307 ms, n = 10), as compared with Kv4.3 alone ($\tau_{inact,CSI}$ = 3178 ± 31 ms, n = 27) (Fig. 5 *F*, *right panel*, and Table 1). KChIP4a accelerated CSI of KChIP4a-2×Kv4.3 complexes ($\tau_{inact,CSI}$ = 2024 ± 95 ms, n = 15), as compared with KChIP4a-2×Kv4.3 alone ($\tau_{inact,CSI}$ = 2354 ± 307 ms, n = 10), whereas KChIP4bl decelerated CSI with $\tau_{inact,CSI}$ at 2885 ± 214 ms (n = 23) for KChIP4a-2×Kv4.3 ($\tau_{inact,CSI}$ = 2354 ± 307 ms, n = 10) (Fig. 5 *F*, *right panel*, and Table 1). These results further confirmed the competitive binding of Kv4.3 between KChIP4a and KChIP4bl for modulation of the channel function, also suggesting that such a variable subunit composition of native Kv4 channel complexes might be subject to altered neuronal excitability in physiological or pathophysiological conditions.

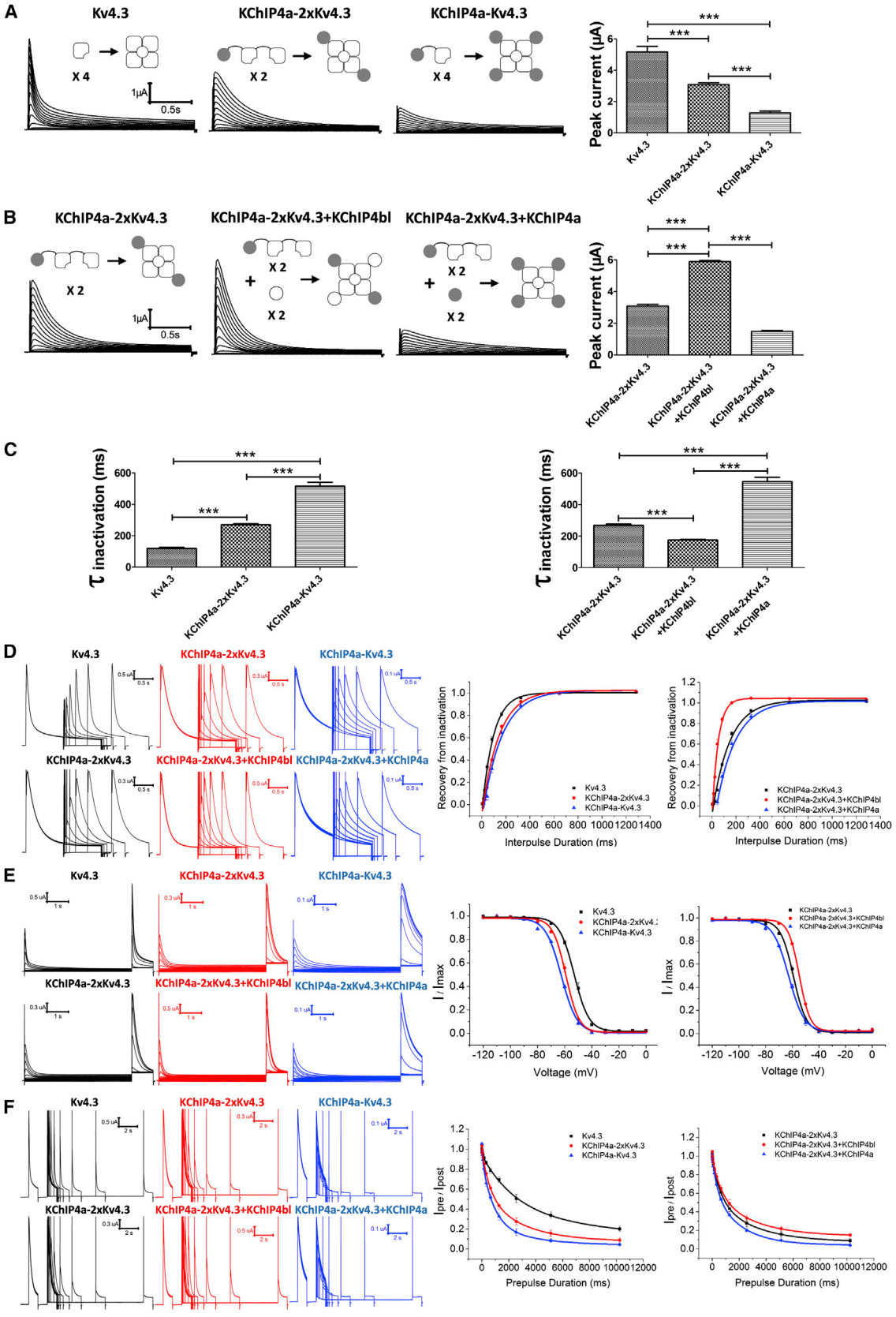

FIGURE 5 Gating properties of Kv4.3-KChIP4 channel complexes. (*A*) Representative current traces and schematic illustrations of Kv4.3, KChIP4a-2×Kv4.3, and KChIP4a-Kv4.3. Outward K^+ currents were evoked by 2-s step depolarization from −100 to +60 mV at 10-mV increments (*left*). Quantitative

(legend continued on next page)

TABLE 1 Gating kinetics of tandem constructs and coexpression with KChIP4a or KChIP4bl

	Inactivation		Recovery		CSI			SSI			Peak Current	
	n	τ (ms)	*n*	τ (ms)	*n*	τ (ms)	Remain	*n*	$V_{1/2}$ (mV)	*K* (mV)	*n*	μA
Kv4.3	30	40.3 ± 2.5	17	94.1 ± 12.3	27	3178.5 ± 30.7	0.201 ± 0.027	30	−53.7 ± 0.9	6.012 ± 0.453	42	5.1 ± 0.3
KChIP4a-Kv4.3	14	624.4 ± 7.8	17	160.1 ± 16.3	12	1956.8 ± 119.1	0.045 ± 0.009	10	−63.3 ± 0.8	5.247 ± 0.487	31	1.2 ± 0.1
KChIP4a-2×Kv4.3	18	269.2 ± 7.3	13	145.2 ± 28.6	10	2354.1 ± 307.4	0.089 ± 0.022	15	−60.6 ± 1.1	5.372 ± 0.632	30	3.0 ± 0.1
KChIP4a-2×Kv4.3 + KChIP4a	15	637.3 ± 7.4	10	160.2 ± 3.4	15	2024.1 ±94.8	0.042 ± 0.013	15	−63.4 ± 0.7	5.788 ± 0.743	20	1.4 ± 0.1
KChIP4a-2×Kv4.3 + KChIP4bl	18	123.6 ± 4.2	20	61.2 ± 6.8	23	2885.2 ± 214.1	0.149 ± 0.015	23	−54.9 ± 0.3	4.541 ± 0.167	24	5.8 ± 0.1

Values are means ± SE; *n* = number of oocytes. Inactivation time constants (τ) of open-state inactivation were obtained by fitting single exponential function (OriginPro version 8.6 software) to the decaying phases of Kv4.3 current evoked by +40-mV depolarization. Time constants (τ) of recovery from inactivation were obtained by fitting a single exponential function to the mean normalized current amplitudes plotted of Kv4.3 current evoked by +40-mV depolarization after a +40-mV prepulse for variable time lengths. Inactivation time constants (τ) of CSI were obtained by fitting a single exponential function to the decaying phases of Kv4.3 current evoked by +40-mV depolarization after a subthreshold −50-mV prepulse with variable durations. Remaining current is the fraction of noninactivated channel current. Mean data points obtained from the SSI protocol with 5-s prepulse were best fitted by a standard single Boltzmann curve, in which $V_{1/2}$ is the half-inactivation potential, and *k* is the slope factor. Peak currents were obtained by measuring peak amplitudes of Kv4.3 current evoked by +40-mV.

DISCUSSION

The goal of this study was to investigate whether different auxiliary KChIPs can compete for heteromultimeric assembly with pore-forming Kv4 α-subunits to form variable channel complexes. Our main findings show that first, distinct KChIP4s can competitively heteroassemble with Kv4-α subunit to modulate channel function; second, the subunit stoichiometry of Kv4-KChIP4s complexes is variable and dependent upon KChIP4 expression level.

Single-molecule subunit counting is a powerful tool for investigating variable subunit stoichiometry of membrane protein without disrupting the membrane environment by counting bleaching steps of fluorescent GFP and mCherry tags. This method has been successfully applied to studying interactions of auxiliary β-subunits with pore-forming α-subunits in fixed mammalian cells (28,36) and triheteromeric NMDA receptors in oocytes (37). In this study, we took advantage of the membrane tethered peptide *k*-ras-CAAX signal (33,34) to anchor Kv4.3-KChIP4s complexes to the plasma membrane and used fixed cells to avoid potential issues of asynchronous photobleaching in the single-molecule subunit counting assay (30). This combination of CAAX signal and fixed-cell approaches allowed us to detect immobile fluorescent spots for competitive heteromultimeric assembly of KChIP4 isoforms with Kv4 α-subunits.

The previous work from ours and others on cocrystal structure reveals that Kv4.3 and KChIP1 form an octameric 4:4 stoichiometry of channel complex in which a single KChIP1 core functions by binding and sequestering Kv4 N-terminus, stabilizing the tetrameric assembly of Kv4 by laterally clamping (31,32). The KChIP core-mediated clamping action on Kv4 further raises the possibility that different KChIPs can competitively bind to Kv4 to form a variable and heteromultimeric Kv4-KChIP channel complex for modulation of the channel function. This hypothesis, however, remains unproved. In this study, we found that the number of KChIP4 proteins in Kv4.3-KChIP4 channel complexes can vary depending on the KChIP4 expression level, consistent with a recent study by Kitazawa et al. (36). This result is also consistent with our previous crystal structure of KChIP4a in which its core domain is identical to KChIP1 core that sequesters Kv4 N-terminus

analysis for peak current amplitudes of Kv4.3 and tandem complexes (n = 30–42 oocytes) (*right*). Values are mean ± SE. Statistical analysis was conducted by Student's *t*-test, and the statistical significance was considered as ***$p < 0.001$. (*B*) Representative current traces and schematic illustrations of KChIP4a-2×Kv4.3, KChIP4a-2×Kv4.3 + KChIP4bl, and KChIP4a-2×Kv4.3 + KChIP4a (*left*). Quantitative analysis for peak current amplitudes of KChIP4a-2×Kv4.3, KChIP4a-2×Kv4.3 + KChIP4bl, and KChIP4a-2×Kv4.3 + KChIP4a (n = 20–30 oocytes) (*right*). Values are mean ± SE; ***$p < 0.001$. (*C*) Quantitative analysis of inactivation time constants for Kv4.3 and tandem complexes (n = 14–30 oocytes) (*left*); quantitative analysis of inactivation time constants for KChIP4a-2×Kv4.3, KChIP4a-2×Kv4.3 + KChIP4bl, and KChIP4a-2×Kv4.3 + KChIP4a (n = 15–18 oocytes) (*right*). Values are mean ± SE; ***$p < 0.001$. (*D*) Representative curves of recovery from inactivation of Kv4.3 and tandem complexes and KChIP4a-2×Kv4.3, KChIP4a-2×Kv4.3 + KChIP4bl, and KChIP4a-2×Kv4.3 + KChIP4a (*left*); quantitative analysis of recovery from inactivation of Kv4.3 and tandem complexes (n = 13–17 oocytes), and KChIP4a-2×Kv4.3, KChIP4a-2×Kv4.3 + KChIP4bl, and KChIP4a-2×Kv4.3 + KChIP4a (n = 10–20 oocytes) (*right*). (*E*) Representative curves of the voltage dependence of SSI of Kv4.3 and tandem complexes and KChIP4a-2×Kv4.3, KChIP4a-2×Kv4.3 + KChIP4bl, and KChIP4a-2×Kv4.3 + KChIP4a (*left*); quantitative analysis of the voltage dependence of SSI of Kv4.3 and tandem complexes (n = 10–30 oocytes) and KChIP4a-2×Kv4.3, KChIP4a-2×Kv4.3 + KChIP4bl, and KChIP4a-2×Kv4.3 + KChIP4a (n = 15–23 oocytes) (*right*). (*F*) Representative curves of CSI of Kv4.3 and tandem complexes and KChIP4a-2×Kv4.3, KChIP4a-2×Kv4.3 + KChIP4bl, and KChIP4a-2×Kv4.3 + KChIP4a (*left*); quantitative analysis of CSI of Kv4.3 and tandem complexes (n = 12–27 oocytes) and KChIP4a-2×Kv4.3, KChIP4a-2×Kv4.3 + KChIP4bl, and KChIP4a-2×Kv4.3 + KChIP4a (n = 10–23 oocytes) (*right*). To see this figure in color, go online.

by clamping (25,31). Our coimmunoprecipitation data provide further evidence that different KChIPs can compete for common KChIP-binding sites in Kv4 by forming heteromeric channel complexes. In single-molecule subunit counting experiments, the increasing amount of KChIP4bl gradually reduces the bleaching steps of GFP for KChIP4a proteins and vice versa. These results indicate that both KChIP4a and KChIP4bl can competitively coassemble with the Kv4.3 channel, and the subunit stoichiometry is variably dependent upon the KChIP4a or KChIP4bl expression level (11,36,38).

The current amplitudes and gating kinetics of native Kv4 channels (both I_{SA} and I_{to}) are determined by the expression levels of auxiliary subunits, such as KChIPs and DPPs (9,11,39–44). Previous studies have shown that coexpression of distinct KChIPs dramatically alters the properties and functional expression of Kv4-encoded currents in native neurons. Because all members of the KChIP family share a high homology in their C-terminal core regions and each KChIP can form two interfaces with two neighboring Kv4 N-terminal domains (3,31,32), this raises the possibility that distinct KChIPs may compete for common KChIP-binding sites in Kv4 channels, resulting in a diverse modulation on Kv4 function. To demonstrate the gating changes of different Kv4.3-KChIP4 channel complexes, we generated two tandem constructs, mimicking the situations of KChIP4a half-occupied channel complexes (KChIP4a-2×Kv4.3) and KChIP4a saturated channel complexes (KChIP4a-Kv4.3). Our recording data show that the effects of KChIP4a on Kv4 gating and current amplitude are more obvious with an increasing number of bound KChIP4a subunits, as compared with groups of Kv4.3, KChIP4a half-occupied and the KChIP4a-saturated group (Fig. 5 and Table 1). We also coexpressed KChIP4a half-occupied, KChIP4a-2×Kv4.3 with KChIP4bl, to mimic channel complex like Kv4.3:KChIP4a:KChIP4bl with the ratio of 4:2:2. The results show that both KChIP4a and KChIP4bl can modulate the function of channel complexes upon coassembly. Similarly, coexpression of KChIP4a-2×Kv4.3 (KChIP4a half-occupied) with KChIP4a results in the function of channel complex similar to the KChIP4a-saturated group, consistent with the single-molecule subunit counting that KChIP4 can assemble with Kv4.3 to form channel complexes in a 4:4 manner. These results show that distinct KChIPs can competitively bind to Kv4 and modulate the channel function.

Neuronal A-type current significantly contributes to physiological repetitive firing and pathogenesis in the brain. Several studies have shown that auxiliary KChIP4 mRNA splicing is neuron-specific and correlates with slow kinetics of A-type current (45). The KChIP4a isoform causes reduced trafficking of Kv4 channels to surface (4,25), impairing the excitatory or inhibitory back-propagating action potentials that ultimately affect neuronal excitability or pain plasticity (46). It has been shown that alternative splicing of neuronal KChIP4 is involved in neurodegenerations, the specific expression or gene-specific alternative splicing shift from KChIP4bl to KChIP4a can lead to an inhibition of Kv4 function and increased secretion of β-amyloid (26). This suggests an involvement of KChIP4 isoform splicing in neurological disorders such as neurodegenerations (26). In summary, our findings show that auxiliary KChIPs can heteroassemble with Kv4 in a competitive manner to form variable Kv4-KChIP4 complexes, likely shaping A-type K^+ channels present at the surface of neurons.

SUPPORTING MATERIAL

One figure is available at http://www.biophysj.org/biophysj/supplemental/S0006-3495(15)00405-1.

AUTHOR CONTRIBUTIONS

J.H.Z., Y.Q.T., and K.W.W. conceived and designed experiments; J.H.Z. and Y.Q.T. performed experiments and analyzed the data; J.H.Z. and Y.Q.T. drafted and K.W.W. finalized the article.

ACKNOWLEDGMENTS

We would like to thank F. Kang and C. Qi for technical assistance and P. Liang for discussion. K.W.W. wishes to thank J. M. Wang for her consistent support during this research.

This work was supported by research grants to K.W.W. from the Ministry of Science and Technology of China (2013CB531302 and 2014ZX09507003-006) and the National Science Foundation of China (31370741 and 81221002).

REFERENCES

1. An, W. F., M. R. Bowlby, …, K. J. Rhodes. 2000. Modulation of A-type potassium channels by a family of calcium sensors. *Nature.* 403: 553–556.
2. Nadal, M. S., A. Ozaita, …, B. Rudy. 2003. The CD26-related dipeptidyl aminopeptidase-like protein DPPX is a critical component of neuronal A-type K+ channels. *Neuron.* 37:449–461.
3. Scannevin, R. H., K. Wang, …, K. J. Rhodes. 2004. Two N-terminal domains of Kv4 K(+) channels regulate binding to and modulation by KChIP1. *Neuron.* 41:587–598.
4. Holmqvist, M. H., J. Cao, …, W. F. An. 2002. Elimination of fast inactivation in Kv4 A-type potassium channels by an auxiliary subunit domain. *Proc. Natl. Acad. Sci. USA.* 99:1035–1040.
5. Cui, Y. Y., P. Liang, and K. W. Wang. 2008. Enhanced trafficking of tetrameric Kv4.3 channels by KChIP1 clamping. *Neurochem. Res.* 33:2078–2084.
6. Liang, P., H. Chen, …, K. Wang. 2010. Functional rescue of Kv4.3 channel tetramerization mutants by KChIP4a. *Biophys. J.* 98:2867–2876.
7. Tang, Y. Q., P. Liang, …, K. Wang. 2013. Auxiliary KChIP4a suppresses A-type K+ current through endoplasmic reticulum (ER) retention and promoting closed-state inactivation of Kv4 channels. *J. Biol. Chem.* 288:14727–14741.
8. Covarrubias, M., A. Bhattacharji, …, G. Wang. 2008. The neuronal Kv4 channel complex. *Neurochem. Res.* 33:1558–1567.
9. Liss, B., O. Franz, …, J. Roeper. 2001. Tuning pacemaker frequency of individual dopaminergic neurons by Kv4.3L and KChip3.1 transcription. *EMBO J.* 20:5715–5724.

10. Rhodes, K. J., K. I. Carroll, …, J. S. Trimmer. 2004. KChIPs and Kv4 alpha subunits as integral components of A-type potassium channels in mammalian brain. *J. Neurosci.* 24:7903–7915.

11. Norris, A. J., N. C. Foeger, and J. M. Nerbonne. 2010. Interdependent roles for accessory KChIP2, KChIP3, and KChIP4 subunits in the generation of Kv4-encoded IA channels in cortical pyramidal neurons. *J. Neurosci.* 30:13644–13655.

12. Hoffman, D. A., J. C. Magee, …, D. Johnston. 1997. K+ channel regulation of signal propagation in dendrites of hippocampal pyramidal neurons. *Nature.* 387:869–875.

13. Bernard, C., A. Anderson, …, D. Johnston. 2004. Acquired dendritic channelopathy in temporal lobe epilepsy. *Science.* 305:532–535.

14. Cai, X., C. W. Liang, …, S. M. Thompson. 2004. Unique roles of SK and Kv4.2 potassium channels in dendritic integration. *Neuron.* 44:351–364.

15. Chen, X., L. L. Yuan, …, D. Johnston. 2006. Deletion of Kv4.2 gene eliminates dendritic A-type K+ current and enhances induction of long-term potentiation in hippocampal CA1 pyramidal neurons. *J. Neurosci.* 26:12143–12151.

16. Kim, J., S. C. Jung, …, D. A. Hoffman. 2007. Regulation of dendritic excitability by activity-dependent trafficking of the A-type K+ channel subunit Kv4.2 in hippocampal neurons. *Neuron.* 54:933–947.

17. Burgoyne, R. D. 2007. Neuronal calcium sensor proteins: generating diversity in neuronal Ca2+ signalling. *Nat. Rev. Neurosci.* 8:182–193.

18. Takimoto, K., E. K. Yang, and L. Conforti. 2002. Palmitoylation of KChIP splicing variants is required for efficient cell surface expression of Kv4.3 channels. *J. Biol. Chem.* 277:26904–26911.

19. O'Callaghan, D. W., B. Hasdemir, …, R. D. Burgoyne. 2003. Residues within the myristoylation motif determine intracellular targeting of the neuronal Ca2+ sensor protein KChIP1 to post-ER transport vesicles and traffic of Kv4 K+ channels. *J. Cell Sci.* 116:4833–4845.

20. Decher, N., A. S. Barth, …, M. C. Sanguinetti. 2004. Novel KChIP2 isoforms increase functional diversity of transient outward potassium currents. *J. Physiol.* 557:761–772.

21. Van Hoorick, D., A. Raes, and D. J. Snyders. 2007. The aromatic cluster in KCHIP1b affects Kv4 inactivation gating. *J. Physiol.* 583: 959–969.

22. Morohashi, Y., N. Hatano, …, T. Iwatsubo. 2002. Molecular cloning and characterization of CALP/KChIP4, a novel EF-hand protein interacting with presenilin 2 and voltage-gated potassium channel subunit Kv4. *J. Biol. Chem.* 277:14965–14975.

23. Jerng, H. H., and P. J. Pfaffinger. 2008. Multiple Kv channel-interacting proteins contain an N-terminal transmembrane domain that regulates Kv4 channel trafficking and gating. *J. Biol. Chem.* 283:36046–36059.

24. Schwenk, J., G. Zolles, …, D. Bentrop. 2008. NMR analysis of KChIP4a reveals structural basis for control of surface expression of Kv4 channel complexes. *J. Biol. Chem.* 283:18937–18946.

25. Liang, P., H. Wang, …, K. Wang. 2009. Structural insights into KChIP4a modulation of Kv4.3 inactivation. *J. Biol. Chem.* 284: 4960–4967.

26. Massone, S., I. Vassallo, …, A. Pagano. 2011. RNA polymerase III drives alternative splicing of the potassium channel-interacting protein contributing to brain complexity and neurodegeneration. *J. Cell Biol.* 193:851–866.

27. Ulbrich, M. H., and E. Y. Isacoff. 2007. Subunit counting in membrane-bound proteins. *Nat. Methods.* 4:319–321.

28. Ji, W., P. Xu, …, L. Chen. 2008. Functional stoichiometry of the unitary calcium-release-activated calcium channel. *Proc. Natl. Acad. Sci. USA.* 105:13668–13673.

29. Nakajo, K., M. H. Ulbrich, …, E. Y. Isacoff. 2010. Stoichiometry of the KCNQ1 - KCNE1 ion channel complex. *Proc. Natl. Acad. Sci. USA.* 107:18862–18867.

30. Plant, L. D., D. Xiong, …, S. A. N. Goldstein. 2014. Individual IKs channels at the surface of mammalian cells contain two KCNE1 accessory subunits. *Proc. Natl. Acad. Sci. USA.* 111:E1438–E1446.

31. Wang, H., Y. Yan, …, J. Chai. 2007. Structural basis for modulation of Kv4 K+ channels by auxiliary KChIP subunits. *Nat. Neurosci.* 10:32–39.

32. Pioletti, M., F. Findeisen, …, D. L. Minor, Jr. 2006. Three-dimensional structure of the KChIP1-Kv4.3 T1 complex reveals a cross-shaped octamer. *Nat. Struct. Mol. Biol.* 13:987–995.

33. Hancock, J. F. 2003. Ras proteins: different signals from different locations. *Nat. Rev. Mol. Cell Biol.* 4:373–384.

34. Choy, E., V. K. Chiu, …, M. R. Philips. 1999. Endomembrane trafficking of ras: the CAAX motif targets proteins to the ER and Golgi. *Cell.* 98:69–80.

35. Hastie, P., M. H. Ulbrich, …, L. Chen. 2013. AMPA receptor/TARP stoichiometry visualized by single-molecule subunit counting. *Proc. Natl. Acad. Sci. USA.* 110:5163–5168.

36. Kitazawa, M., Y. Kubo, and K. Nakajo. 2014. The stoichiometry and biophysical properties of the Kv4 potassium channel complex with K+ channel-interacting protein (KChIP) subunits are variable, depending on the relative expression level. *J. Biol. Chem.* 289:17597–17609.

37. Ulbrich, M. H., and E. Y. Isacoff. 2008. Rules of engagement for NMDA receptor subunits. *Proc. Natl. Acad. Sci. USA.* 105:14163–14168.

38. Holmqvist, M. H., J. Cao, …, W. F. An. 2001. Kinetic modulation of Kv4-mediated A-current by arachidonic acid is dependent on potassium channel interacting proteins. *J. Neurosci.* 21:4154–4161.

39. Kuo, H. C., C. F. Cheng, …, K. R. Chien. 2001. A defect in the Kv channel-interacting protein 2 (KChIP2) gene leads to a complete loss of I(to) and confers susceptibility to ventricular tachycardia. *Cell.* 107:801–813.

40. Panama, B. K., D. Latour-Villamil, …, P. H. Backx. 2011. Nuclear factor kappaB downregulates the transient outward potassium current I(to,f) through control of KChIP2 expression. *Circ. Res.* 108:537–543.

41. Jeyaraj, D., S. M. Haldar, …, M. K. Jain. 2012. Circadian rhythms govern cardiac repolarization and arrhythmogenesis. *Nature.* 483: 96–99.

42. Jerng, H. H., P. J. Pfaffinger, and M. Covarrubias. 2004. Molecular physiology and modulation of somatodendritic A-type potassium channels. *Mol. Cell. Neurosci.* 27:343–369.

43. Jerng, H. H., K. Kunjilwar, and P. J. Pfaffinger. 2005. Multiprotein assembly of Kv4.2, KChIP3 and DPP10 produces ternary channel complexes with ISA-like properties. *J. Physiol.* 568:767–788.

44. Maffie, J., and B. Rudy. 2008. Weighing the evidence for a ternary protein complex mediating A-type K+ currents in neurons. *J. Physiol.* 586:5609–5623.

45. Baranauskas, G. 2004. Cell-type-specific splicing of KChIP4 mRNA correlates with slower kinetics of A-type current. *Eur. J. Neurosci.* 20:385–391.

46. Hu, H. J., Y. Carrasquillo, …, R. W. Gereau, 4th. 2006. The kv4.2 potassium channel subunit is required for pain plasticity. *Neuron.* 50:89–100.